Water Reuse

Water Reuse Vol 16 No 1, 69 doi: 10.2166/wrd.2026.094

Water and ammonium recovery from the digestate of short-fiber residues in paper recycling mills using membrane filtration and natural zeolite

Dheeraja Winter [a,b,*], Jerome Bährens[a], Beate Förster [c], Jürgen Pettrak [a], Simone Krafft [a], Markus Grömping [a] and Silvio Beier[b]

[a] Institute NOWUM-Energy, FH Aachen, University of Applied Sciences, Heinrich-Mussmann-Str. 1, Juelich 52428, Germany
[b] Department of Civil Engineering, Bauhaus University of Weimar, Wielandstraße 2, Weimar 99421, Germany
[c] Ernst Ruska-Centre for Microscopy and Spectroscopy with Electrons, Forschungszentrum Juelich GmbH, Wilhelm-Johnen-Straße, Jülich 52428, Germany
*Corresponding author. E-mail: d.winter@fh-aachen.de

DW, 0000-0001-6752-3322; BF, 0000-0002-8464-4473; JP, 0009-0004-6577-0206; SK, 0000-0003-0357-4379; MG, 0009-0005-3696-7963

ABSTRACT

This study investigates nanofiltration (NF) and reverse osmosis (RO) treatment of the liquid fraction from digestate of short-fiber residues from paper recycling mills, focusing on water reuse and ammonium (NH_4-N) recovery. NF removed up to 86% chemical oxygen demand (COD) and fully retained phosphorus (P_{tot}), but separated only 40–55% of total nitrogen (N_{tot}) and NH_4-N. RO performed better, removing 96% COD, 86% NH_4-N and N_{tot}, while fully retaining P_{tot}. RO permeate met the freshwater quality for paper recycling, with small NH_4-N remaining. To improve NH_4-N recovery, natural zeolite was tested with RO in three scenarios: treating the liquid fraction of digestate, RO retentate, and RO permeate. The highest NH_4-N adsorption (79%, 7.8 mg/g) occurred with RO retentate, and the highest desorption (53%, 2.9 mg/g) with RO permeate. Adsorption performance varied with NH_4-N concentration and pretreatment, with higher NH_4-N levels leading to greater adsorption. COD was also reduced by up to 70% during adsorption. RO treatment of digestate in a model paper mill (0.7 Mt/year production capacity) could recover about 38,000 m^3 of water annually, saving 71,000 €. Combined savings from water reuse and avoided digestate disposal could alone reach 0.2 million € annually.

Key words: ammonium recovery, digestate, membrane filtration, short-fiber residues, water reuse, zeolite

HIGHLIGHTS

- Reverse osmosis-treated digestate from short-fiber residues largely meets water quality standards for paper recycling.
- Recovered water can replace up to 6% of freshwater in a model paper mill.
- Scanning electron microscopic images reveal minimal scaling and fouling, but considerable particle-membrane interactions on the membrane.
- First study applying natural zeolite to this type of digestate from short-fiber residues.
- Zeolite adsorption linked to NH_4-N concentration in the treated stream.

GRAPHICAL ABSTRACT

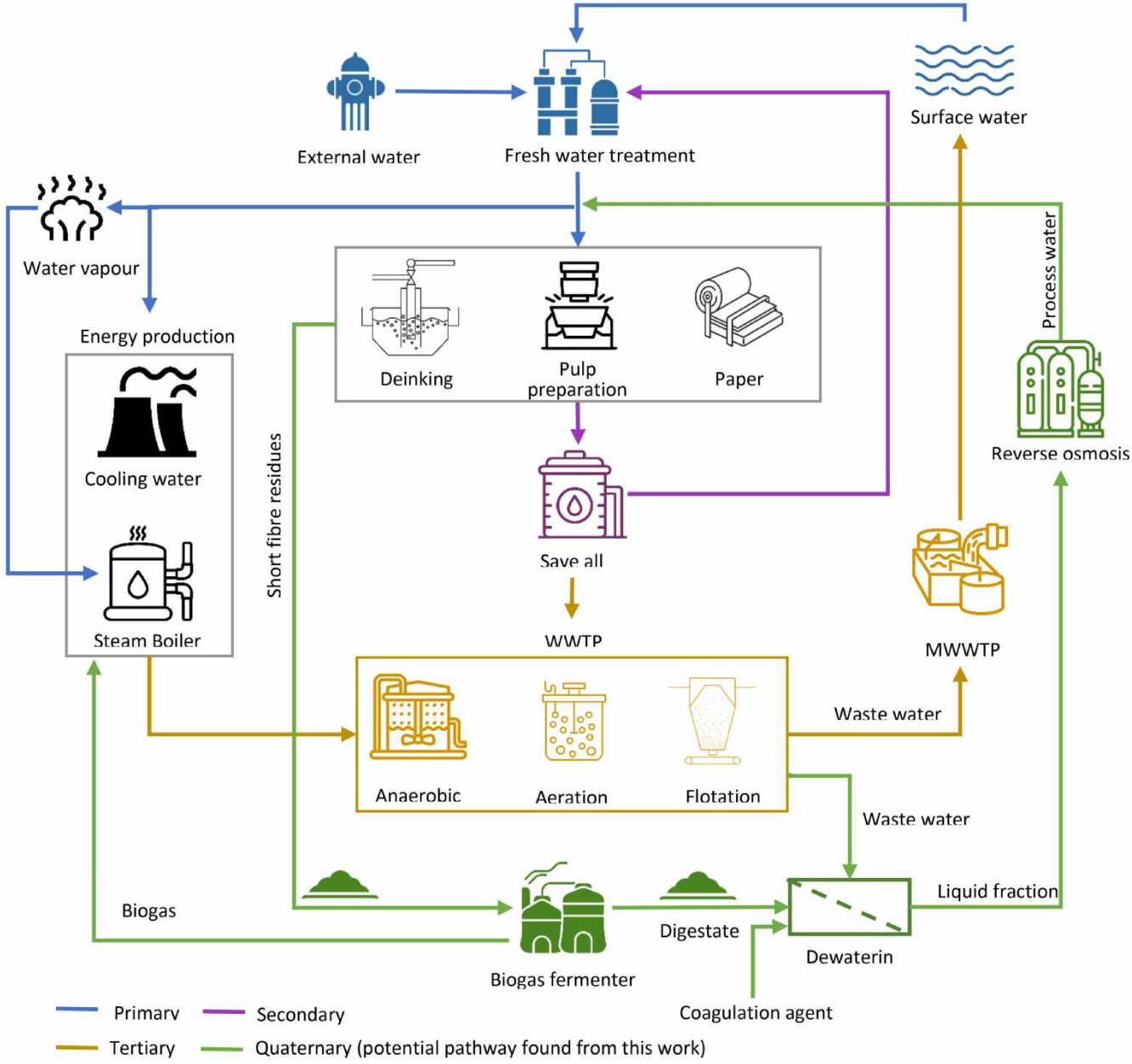

1. INTRODUCTION

The paper industry ranks among the top five energy-intensive sectors globally, and Germany is the fourth largest industrial sector in terms of production volume, which accounts for about 25.2% of European paper and board production as of 2023 and 25% of Europe's consumption as of 2021 (CEPI 2021, 2024). Germany achieved a 99.8% recycling rate for paper and cardboard packaging in 2021 (Cayé *et al.* 2021). Despite sustainability benefits, paper recycling consumes an average of 2.5 kWh/kg of paper. With 79% of paper production in Germany based on recycled waste paper, residue generation during recycling has increased (German Federal Environment Agency 2022). Recycling generates various residues, including organic short-fiber wastes and inorganic components (e.g., mineral pigments and calcium carbonate). Short-fiber residues are one of those residues produced during paper recycling that include deinking sludge, pellet sludge, and fiber sludge. Paper can be reused in the recycling process up to 20 times, but short-fiber residues become too weak for reuse. In 2013,

waste distribution in Germany's paper industry included 19% deinking sludge and 48% fiber waste, mostly incinerated or landfilled in some countries (Faubert *et al.* 2019).

Anaerobic digestion of these short-fiber residues yields biogas with the potential to reduce greenhouse gas emissions compared with fossil fuels (Giuntoli *et al.* 2015). The EU aims for carbon neutrality by 2050, with Germany targeting 80% renewable energy share (EEA 2022). Continuous biogas production from short fiber residues has been demonstrated at lab and pilot scales, with biogas yields reported up to 400 NL/kg organic dry matter (oDM) from various types of short fiber residues such as deinking sludge (Steffen *et al.* 2017; Amare *et al.* 2019; Bareha *et al.* 2022). Digestate from these short fiber residues contains 70–90% water, with nutrients such as total nitrogen (N_{tot}) and phosphorus (P_{tot}). However, the direct use of this digestate is prohibited due to its complex composition and strict regulatory constraints (German Federal Office of Justice 2019). Mismanagement of digestate can cause environmental issues like eutrophication and ammonia emissions, leading to soil fertilization limits of 170 kg N/(ha·year). Additionally, recent findings by the German Federal Environment Agency have highlighted serious per- and polyfluoroalkyl substances (PFAS) contamination incidents in Germany, such as in Arnsberg, Möhnetalsperre, and Rastatt. These contaminations arose from the illegal use of paper industry sewage sludge as fertilizer, leading to PFAS pollution of approximately 700 hectares of farmland and groundwater. This has resulted in the closure of drinking water wells, increased water treatment costs, and forced destruction of crops due to PFAS presence in food plants. Such events imply the critical need for proper digestate management to avoid persistent organic pollutant contamination.

Many studies have demonstrated the biogas potential of short-fiber residues for energy recovery. However, the treatment and further utilization of the resulting digestates have not been addressed to date. Recovering water from these digestates presents an opportunity to reduce freshwater consumption and wastewater discharge in paper recycling mills. Previous work of Cheenakula *et al.* (2025) characterized digestate from short-fiber residues and explored preliminary ultrafiltration (UF) treatment. Challenges were identified in meeting water quality standards for immediate reuse in paper mills, necessitating further treatment, either through downstream processes or by replacing UF with nanofiltration (NF) or reverse osmosis (RO). Therefore, this study focuses on treating the liquid fraction of the digestate from short fiber residues using NF and RO. The main objective of this study is to reduce and concentrate nutrients and contaminants, such as chemical oxygen demand (COD), to recover process water that meets the quality standards for reuse in paper recycling mills. Additionally, a preliminary economic assessment was conducted in this study to evaluate the necessity of water recovery from these digestates. The assessment also aimed to estimate potential freshwater savings and economic benefits from integrating these treatment methods into mill water management systems.

Concurrently, this study investigates the use of natural clinoptilolite for ammonium (NH_4-N) recovery from this digestate as part of a hybrid technology combining zeolite adsorption with RO, enabling simultaneous nutrient recovery and water purification. Recovering NH_4-N helps to reduce nutrient-related environmental impacts and supports circular nutrient use in the paper recycling sector. Natural zeolite is a low-cost and sustainable sorbent and has been applied for heavy metals, antibiotics, and pathogens (Al Dwairi *et al.* 2015; Omar 2015; Ma *et al.* 2018; Zhang *et al.* 2019). Recent studies demonstrated NH_4-N recovery from several wastewaters, such as municipal wastewater, greywater, dairy wastewater, urine, and landfill leachate (Aydın Temel & Kuleyin 2016; Tarpeh *et al.* 2017; Wasielewski *et al.* 2017; Kotoulas *et al.* 2019; Guida *et al.* 2020; Maghfiroh *et al.* 2023; Zhang *et al.* 2024). In biogas systems, clinoptilolite has been used mainly for agricultural digestates (Hajduk *et al.* 2017; Wasielewski *et al.* 2017; Leca *et al.* 2024). Wasielewski *et al.* (2017) reported up to 70% NH_4-N adsorption using a dosage of 0.1 g clinoptilolite per 1 mg NH_4-N in high-strength CSTR wastewater.

However, no study has examined clinoptilolite for digestate derived from short-fiber residues in paper recycling. This digestate contains mineral pigments, elevated Ca^{2+} and Mg^{2+}, organic matter and additives typical for the paper industry. These constituents may block exchange sites, compete with NH_4^+ or modify surface charge and dynamics of ion exchange. Therefore, we hypothesize that the ion-exchange performance of clinoptilolite would be influenced by this complex matrix, and that high Ca^{2+}, Mg^{2+}, pigments and organic matter may significantly inhibit or alter NH_4^+ adsorption compared with synthetic or agricultural digestates.

Manufacturer data indicate high NH_4^+ affinity under low-ionic-strength conditions, but zeolite behavior in complex industrial digestates remains uncertain. This study, therefore, investigates how matrix constituents influence NH_4-N adsorption at a similar dosage comparable to the study by Wasilewski *et al.* (2017). Clinoptilolite was evaluated in three scenarios: (1) treating the liquid fraction of digestate before RO, (2) treating the RO concentrate to recover more NH_4-N and water, and (3) treating the RO permeate to improve water quality for reuse in paper recycling.

2. METHODS

2.1. Digestate

For the experimental study in the present work, digestates of paper recycling residues from lab as well as pilot-scale anaerobic fermenters were investigated. The lab-scale anaerobic fermenters (70 L, 50 rpm, residence time 50 days) are fed with short-fiber residues such as deinking sludge, short-fiber sludge, and pellet sludge from German paper mills and are operated at the Institute of NOWUM-Energy, Aachen University of Applied Sciences, Germany. The operation of the pilot-scale fermenter and the composition of both lab- and pilot-scale digestates were as described in the previous publication (Cheenakula *et al.* 2025).

2.2. Experimental set-up

2.2.1. UF, NF, and RO

In this study, the liquid fraction of the pilot-scale digestate was used as the feed for batch filtration using flat-sheet membranes for UF, NF, and reverse RO. From here on, the term feed refers to the liquid fraction of the digestate, in accordance with membrane filtration terminology. The batch tests were conducted using a laboratory-scale filtration unit (Minimem, PS Prozesstechnik GmbH) with a membrane area of 0.0117 m^2. The dewatering method of the digestate, along with the experimental setup of the membrane filtration system, including plant design, operating protocol of the batch tests, and membrane cleaning procedure, has been described in the previous publication (Cheenakula *et al.* 2025). Cleaning after the batch tests involved manual removal of the accumulated cake, flushing of the membrane under tap water (5 min), chemical cleaning by pumping 50% ethanol through the membrane module (10 min), and final pumping of distilled water (5 min) to remove the traces of ethanol. The filtration unit is not designed for backwash. All batch tests were performed in triplicate. The operating parameters and membrane specifications for each filtration type are summarized in Table 1. Feed at the start and permeate and retentate at the end of each batch test were taken for analysis.

2.2.2. Hybrid zeolite and RO approach

Three scenarios were evaluated for NH_4-N recovery using zeolite and RO, as shown in Figure 1. In Scenario 1, the liquid fraction obtained after solid–liquid separation of digestate was treated with zeolite before RO. In Scenario 2, the liquid fraction was first subjected to RO, and the resulting concentrate was treated with zeolite, while in Scenario 3, the permeate was treated with zeolite.

Table 1 | Process parameters during the batch tests of UF

Filtration	Membrane type	Series	MWCO (Da)	Supplier	pH (–)	Pressure (bar)	Temperature (°C)	Rejection
UF	PES	MT Series	5,000	Synder filtration	7.5–8.0	2–4	20	–
NF	PES	DK series	150–300	Suez	7.5–8.0	8–10	20	98% $MgSO_4$
RO	PA	AD series	Approximately 100	Suez	7.5–8.0	10–12	20	99.8% NaCl

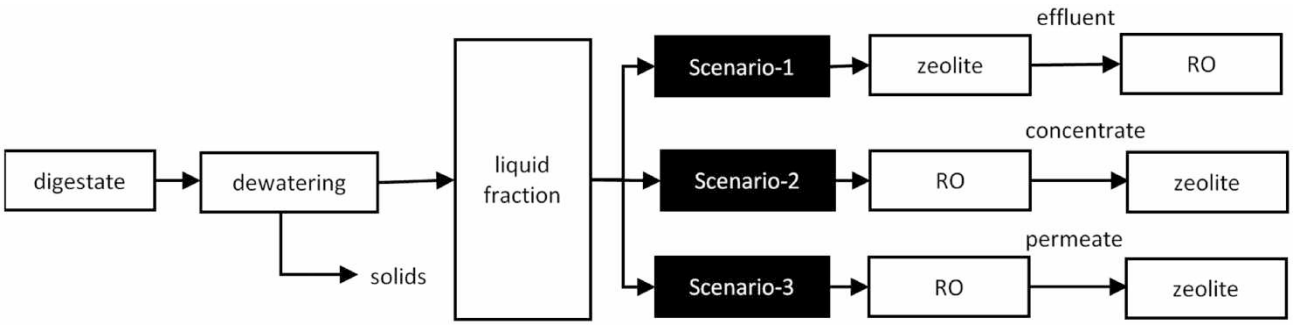

Figure 1 | Flowchart of the hybrid zeolite–RO treatment scenarios.

Jar tests were conducted in triplicate using natural zeolite (Clinoptilolite, 84% purity, effective pore diameter: 0.44 nm, natural zeolite fein B, Fulminant GmbH, Germany). Each test was performed in a 0.6 L glass beaker. Zeolite was added at a dosage of 0.1 g per 1 mg NH_4-N available in the treated stream. This dosage was chosen based on the manufacturer's cation-exchange capacity (1.20–1.50 mol/kg) and intentionally exceeded the theoretical NH_4^+ binding capacity to account for competing cations. The mixture was stirred (50 rpm) at room temperature for 20 h to facilitate NH_4-N adsorption. It was followed by a decanting stage to separate the zeolite through centrifugation.

The separated zeolite from the adsorption stage was subjected to a desorption (regeneration) process. Regeneration was performed using NaCl regenerant solution with a 30-fold molar excess relative to the estimated NH_4-N bound available after the adsorption stage in each scenario. This resulted in different scenario-specific regenerant strengths: 46.5 g/L NaCl in Scenario 1, 204 g/L in Scenario 2, and 5 g/L in Scenario 3, corresponding to NaCl-to-NH_4-N ratios (mg NaCl/mg NH_4-N) of 0.148, 0.703, and 0.053 N, respectively. The zeolite was suspended in the regeneration solution, stirred for 20 h at room temperature, and decanted to separate the zeolite. The supernatants from both adsorption and desorption stages were sampled to determine NH_4^+-N removal efficiency, estimate NH_4-N uptake by the zeolite, and quantify the recovered NH_4-N in the form of ammonium chloride (NH_4Cl).

The liquid fraction from the digestate was separated in all scenarios as described in the previous publication (Cheenakula *et al.* 2025). In Scenario 2, the concentrate was produced using a pilot-scale RO unit equipped with a 0.5 L feed container, as illustrated in Figure S1 in the Supplementary material. This unit employed a spiral-wound membrane module (<300 Da, ULP 2012, 150 GPD, Vontron®), operated at 25 °C and 8 bar. The permeate in Scenario 3 was generated using the flat-sheet RO membrane MiniMem lab-scale plant, as described in Table 1.

2.3. Analytical methods

All the samples generated in this study, including digestates, the liquid fractions from the digestate, i.e., feed, permeate, and retentate, and the samples from the zeolite experiments, were analyzed at FH Aachen. N_{tot} (LCK 238), NH_4-N (LCK 303), P_{tot} and PO_4-P (LCK 350, LCK 349), COD (LCK 380), TOC (LCK 303), hardness, Ca^{2+} and Mg^{2+} (LCK 327) were measured using cuvette kits and the DR2800 photometer from Hach Lange®, Düsseldorf. pH and electrical conductivity (EC) were analyzed using electrodes from Greisinger® (DIN EN ISO 10523-C5) and Hanna Instruments® (DIN EN 27888), respectively. The determination of dry matter (DM), oDM, and suspended solids was carried out according to respective DIN standards.

The morphology of the membrane and the structure of the fouling, as well as the surface of fresh zeolite and the zeolite after adsorption and desorption, were observed and analyzed using a Thermo Fisher Volumescope (FEG), which was equipped with an EDAX Octane Elect EDS detector. The membrane samples were mounted on standard pin stubs and coated with a 20 nm carbon layer to ensure EC, while the zeolite samples were coated with a 25 nm carbon layer.

2.4. Formulas

Nutrient retention (NR) is defined as:

$$\mathrm{NR}\% = \frac{(C_f \cdot V_f) - (C_p \cdot V_p)}{C_f \cdot V_f} \tag{1}$$

here C_f is the nutrient concentration in feed at the start of the cycle (mg/L); C_p is the nutrient concentration in permeate at the end of the cycle (mg/L); V_f is the volume of feed at the start of the cycle (L); V_P is the volume of permeate at the end of cycle (L).

Permeate flux (J) is defined as:

$$J = \frac{Q}{A} \tag{2}$$

here J is the permeate flow (L/(m^2·h)); Q is the volume flow of the permeate (L/h); and A is the membrane surface area (m^2).

Flux recovery rate (FRR) is defined as:

$$\text{FRR}\ (\%) = \left(1 - \frac{J_{\text{PWM}}}{J_o}\right) \cdot 100 \tag{3}$$

here J_{PWM} is the $_{\text{p}}$ermeate flux of pure water after the UF cycle following membrane wash [L/(m^2·h)] and J_o is the initial permeate flux of pure water by the membrane before the cycle (L/(m^2·h)).

The pure water permeability (PWP) was calculated by the ratio of the pure water flux (J_{PW}) to the applied pressure (TMP):

$$\text{PWP}\left(\frac{L}{\text{m}^2 \cdot \text{h} \cdot \text{bar}}\right) = \frac{J_{\text{PW}}}{\text{TMP}} \tag{4}$$

The amount of NH_4-N adsorbed onto the zeolite is calculated based on the concentration difference between the treated influent and the effluent after the adsorption process:

$$NH_4\text{-N}_{\text{adsorbed}} = NH_4\text{-N}_{\text{influent}} - NH_4\text{-N}_{\text{effluent}} \tag{5}$$

The amount of NH_4-N desorbed from the zeolite is determined by calculating the difference between the total NH_4-N adsorbed (i.e., available for desorption) and the NH_4-N measured in the solution (NH_4Cl) after desorption:

$$NH_4\text{-N}_{\text{desorbed}} = NH_4\text{-N}_{\text{adsorbed}} - NH_4\text{-N}_{\text{retained}} \tag{6}$$

3. RESULTS AND DISCUSSION

3.1. Separation efficiencies

This study builds upon the findings presented in the previous work (Cheenakula *et al.* 2025), where UF achieved removal efficiencies of up to 62% for COD, and significant reductions in N_{tot} (37%), NH_4-N (25%), P_{tot} (65%), and PO_4-P (49%). While these results showed the potential of UF for partial treatment, the permeate quality did not meet the reuse standards for process water in paper recycling mills. To address this, the current study evaluates the performance of NF and RO processes for the treatment of the liquid fraction of digestate, aiming to fulfil the quality requirements for water reuse in the paper recycling mill. Due to the limitations of UF (5,000 Da) in separating dissolved compounds from the feed stream, NF and RO membranes with a MWCO $\leq$ 300 Da were selected to achieve higher separation efficiencies. PES membrane was used for NF, while PA membrane was employed for RO, due to their proven chemical resistance and selectivity in treating complex wastewater matrices.

To enable economic feasibility on an industrial scale, the NF and RO processes were investigated individually rather than in combined stages of filtration. Figure 2 shows the separation efficiencies of COD, N_{tot}, NH_4-N, P_{tot} and PO_4^{3-}-P, achieved

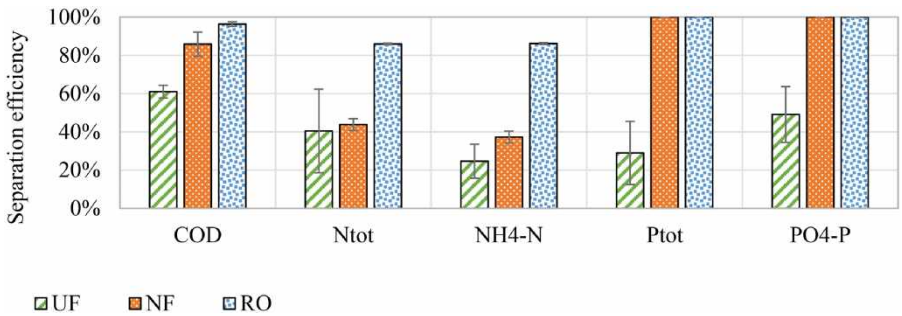

Figure 2 | Separation efficiencies of COD, N_{tot}, NH_4-N, P_{tot}, and PO_4-P by UF, NF and RO, respectively.

through the NF and RO processes. The permeate quality data for UF, NF, and RO are presented in the upcoming section for comprehensive comparison with quality requirements for reuse in a paper recycling mill.

In this study, NF and RO achieved COD separation efficiencies of up to 86 and 96%, respectively. These results align with available literature on the treatment of liquid fractions of digestate and industrial and municipal wastewaters using membrane technologies. A full-scale study conducted by Digested Organics LLC (2020) in Michigan at a food waste digester facility with a capacity of 100,000 GPD demonstrated the feasibility of RO for this application. A three-stage RO process achieved over 99.9% COD separation, while a separate two-stage RO setup reported a 97% separation efficiency, reducing COD levels from 800 to 22 mg/L. Hafiz *et al.* (2021) investigated tertiary-treated municipal wastewater for reuse in irrigation and reported that NF achieved 68% COD removal with a final concentration of 20 mg/L, while RO achieved 87% removal, reducing COD to below 8 mg/L. Zielińska & Mikucka (2021) treated digestate from anaerobic treatment of distillery stillage using RO and observed COD removal efficiencies exceeding 90%, with final concentrations around 80 mg/L. Similarly, Gienau *et al.* (2018) conducted pilot-scale NF tests on anaerobic sludge at a 2.5 MWe biogas plant and achieved significant nutrient retention, although with comparatively moderate COD reduction (~70%), owing to the larger pore sizes typical of NF membranes. In comparison, the current study achieved 86 and 96% COD removal through NF and RO, reducing the levels to 106 and 41 mg/L, respectively. These outcomes in the current study reflect the high efficiency of RO in treating the liquid fraction of digestate derived from short-fiber residues in paper recycling processes, despite the complex matrix. NF offers partial purification, but it falls short of achieving the water quality needed for reuse.

Despite the significantly larger MWCO (5,000 Da) of the UF compared with the NF (300 Da), the UF achieved a N_{tot} separation of 40%, while the NF showed a slightly higher separation of 44%. Similarly, the UF achieved a 25% separation of NH_4-N, compared with 37% by the NF. This suggests that the separation in UF is not purely size-based. It is hypothesized that N-containing complexes may form or interact with organic and colloidal foulants. Huang *et al.* (2023) observed that NF membranes treating UF permeate from biogas-slurry developed dense organic-rich contamination layers. These layers contained macromolecular N-compounds, which contributed to unexpected N retention. These interactions could increase the apparent size of N-species and hinder passage through the membrane. Concentration polarization at the membrane surface may also enhance local ammonium concentration. It enhances diffusive back-transport and reduces apparent rejection. Fouling layers or organic deposits may block pores and interact with NH_4-N, contributing to partial retention. Recent work by Foorginezhad *et al.* (2025) emphasizes that real wastewater treatment must account for complex interactions between solutes, fouling layers, and membrane surface charge.

Both the UF and NF membranes in the current study are PES-based. The lower surface charge density of PES limits its electrostatic repulsion against small, positively charged ions like NH_4^+, resulting in lower separation rates compared with NF for this specific ion. Additionally, even with a larger MWCO, UF can still achieve the separation of a portion of nitrogen-containing organic macromolecules, contributing to the overall N_{tot} separation. In contrast, the PA-based RO membrane achieved higher N_{tot} and NH_4-N rejection (both 86%). The similar separation rates for N_{tot} and NH_4-N in the RO process indicate that the majority of the N_{tot} in the digestate is in the form of dissolved NH_4-N. The increased performance of PA-based RO membrane in this study can be explained by its highly cross-linked polyamide structure, which forms a dense and selective active layer, effectively rejecting small, charged ions like NH_4^+ despite having a similar MWCO range (150–300 Da) as the NF. In the study of Mai *et al.* (2025), separation efficiencies above 95% are reported using a PA-based RO membrane for rare earth wastewater containing high NH_4-N concentrations up to 5,000 mg/L. Similarly, Anari *et al.* (2023) observed NH_4-N separation efficiencies exceeding 95% using a PA-based RO membrane from DOW FilmTec, Minneapolis, MN, for the treatment of synthetic wastewater containing NH_4-N concentrations up to 1,000 mg/L. Unlike PA-based membranes, the PES-based membranes used in this study, while also designed for tight separation, generally have a more open pore structure and lower charge density, which can reduce their ability to reject monovalent ions. However, PA membranes typically possess a negatively charged surface due to the presence of functional groups such as carboxyl (–COOH) and amine ($–NH_2$) groups. These groups can ionize depending on the pH value of the solution, leading to a net negative or positive surface charge that enhances the electrostatic repulsion of negatively or positively charged ions like NH_4^+, thereby improving separation rates. This characteristic makes the PA membrane particularly effective for separating dissolved ionic species. However, Fujioka *et al.* (2019) found a phenomenon that compounds with more N-atoms tend to have lower rejection rates, likely due to hydrogen bonding interactions between the N-atoms and the amide groups in PA membranes, which can facilitate their passage. This phenomenon can be possibly prevented by increasing the pH of the solution to increase negatively charged functional groups on the PA membrane. Liu *et al.* (2025) used molecular dynamics simulations to

investigate solute transport through charged PA membranes. Their study showed that the retention of symmetrical salts improves at both high and low pH, while for asymmetrical salts, retention depends on the ion with the higher charge valency. This behavior is explained by the coupling of cations and anions, which are either sterically repelled or attracted by the membrane's charge, leading to ion clustering. Increasing the concentration of charged functional groups on the membrane surface enhances ion rejection, particularly for ions with higher valency, which in turn improves the rejection of their co-ions. The simulations of Liu *et al.* (2025) further suggested that counter-ions associate with oppositely charged functional groups, while co-ions are repelled by groups of the same charge. This implies that at high pH, the presence of negatively charged COO^- groups on the membrane surface increases salt rejection. However, their experimental results showed the highest retention at low pH, highlighting the complex interplay between membrane charge and solute retention.

The 100% separation efficiencies for P_{tot} and PO_4-P were observed in both the NF and RO processes in the current study. It indicates that the P in digestate is predominantly present in the form of particulate-bound phosphates, polyphosphates, or organic phosphorus compounds, which are substantially larger and less soluble than NH_4^+ ions. Consequently, these larger P-compounds are inherently easier to retain, even by membranes with slightly larger pore sizes or looser structures, irrespective of PES and PA membranes. Having said that, the UF membrane in this study only achieved 29% separation for P_{tot}, reflecting its inability to retain smaller, dissolved P-species effectively. In digestates from paper mill wastewater, P compounds are often present as low molecular weight species like glucose-6-phosphate (260 Da), and adenosine monophosphate (347 Da) (Leiviskä *et al.* 2008). These small, soluble compounds can easily permeate UF membranes with a 5,000 Da MWCO, leading to low retention rates. In the study by Anari *et al.* (2023) on pressure-driven membrane nutrient preconcentration for downstream electrochemical struvite recovery, the performance of various membranes was evaluated and reported P separation rates ranging from 90 to 100% across these different membrane materials. High P separation is less dependent on the specific membrane material and more influenced by the characteristics of the P-species present in the feed stream, as well as the pore size of the membrane. Additionally, PO_4^{3-} ions carry a higher negative charge density compared with the monovalent NH_4^+ion, leading to stronger electrostatic repulsion within the negatively charged layers of membranes. This charge effect, combined with size exclusion, likely contributes to the complete retention of P-compounds in both RO and NF membranes with lower MWCO, aligning with the principle that membranes generally perform better at rejecting multivalent ions than monovalent ions.

3.2. Membrane performance

The permeate flux profiles during the 120-min batch filtration of the liquid fraction of digestate revealed distinct behaviors for UF, NF, and RO membranes (Figure 3(a)). Initially, NF demonstrated the highest flux at 22 L/(m^2·h), followed by UF at 15.8 L/(m^2·h) and RO at 3.8 L/(m^2·h). In the literature, PES-based UF membranes with a MWCO around 5,000 Dalton have demonstrated permeate fluxes ranging from approximately 15 L/(m^2·h) at 1 bar to about 40 L/(m^2·h) at 4 bar while treating polymer-flooding produced water and laundry wastewater, respectively (Liu *et al.* 2016; Kaya & Dayanir 2020). For PES-based NF membranes, flux values typically range between 12 and 25 L/(m^2·h) under pressures from 6 to 15 bar when treating tertiary treated municipal wastewater and industrial wastewater, respectively (Cséfalvay *et al.* 2008; Hafiz *et al.* 2021).

PA-based RO membranes, despite operating at high pressures (10–30 bar), typically exhibit lower permeate fluxes due to their dense selective layers. In this study, fluxes ranged from 3.0 to 3.8 L/(m^2·h) when treating the liquid fraction of short fiber digestate at 10–12 bar. Preliminary work for this study involved a three-stage filtration system (UF → NF → RO). The liquid fraction of short-fiber digestate was first treated by UF, followed by NF treating the UF permeate, and RO treating the NF permeate at 24 bar. In this setup, RO achieved a flux of 21.4 L/(m^2·h) when operating at 24 bar (Figure S2 in the Supplementary material). This demonstrates that higher operating pressure combined with improved feed quality increases RO throughput. Higher permeate flux enhances water recovery but also increases energy consumption. Moreover, the UF and NF pre-treatment required for higher RO flux adds further operational energy and capital costs. By contrast, Adam *et al.* (2018) reported significantly higher fluxes of 12–15 L/(m^2·h) at 30 bar for industrial digestate. The three-stage RO system in the preliminary experiments of this current study achieved higher flux than the RO treating the liquid fraction of short-fiber digestate. These observations highlight the strong influence of both pressure and feed pre-treatment. Low-pressure operation limits flux and permeate production but reduces energy input. In contrast, higher-pressure operation increases throughput, but at the expense of higher energy use and additional pre-treatment costs.

Despite the larger MWCO of the UF membrane (5,000 Da) in this study, its initial flux was lower than that of NF. This difference might be primarily due to the operational modes. UF was operated in dead-end mode, whereas NF employed

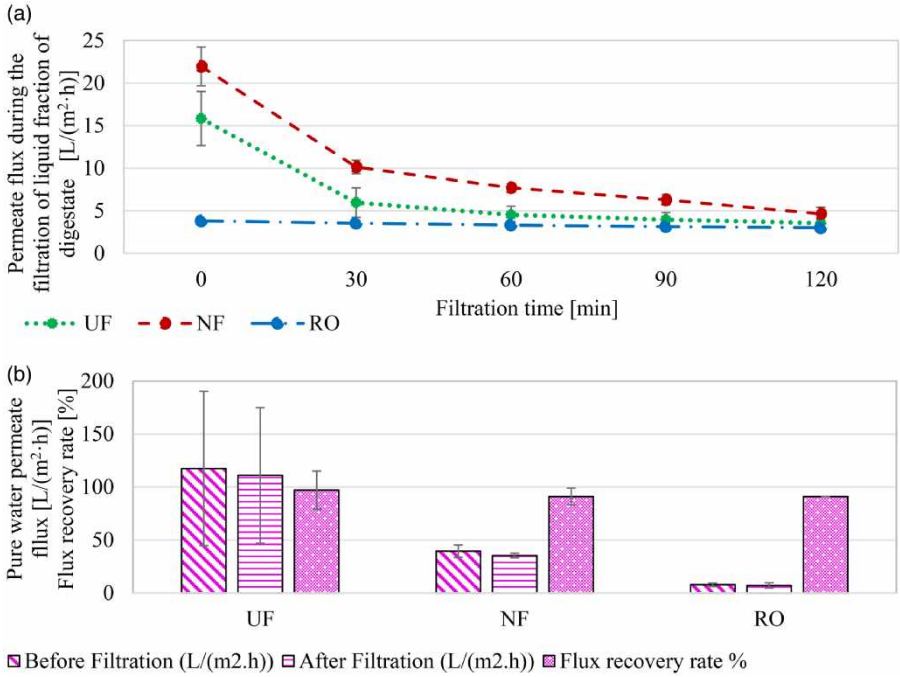

Figure 3 | (a) Permeate flux of UF, NF, and RO during the filtration of liquid fraction of digestate from short fiber residues, (b) Pure water: permeate flux and flux recovery rate of UF, NF, and RO.

cross-flow filtration. It is well-known that dead-end filtration encourages rapid particle deposition and cake layer formation on the membrane surface, resulting in fouling, whereas cross-flow filtration continuously sweeps the membrane surface, preventing fouling by reducing cake build-up. A very thick cake layer formation on the UF membrane postfiltration is seen in Figure S2 in the Supplementary material. Such rapid fouling is a well-known phenomenon in dead-end filtration, especially when treating feeds rich in suspended solids and organic matter. But the feed in this study contained low suspended solids (<0.2 mg/L). The elevated concentration of calcium ions (Ca^{2+}), approximately 200 mg/L, might have accelerated the fouling. Liu *et al.* (2016) reported that Ca^{2+} promotes fouling by increasing adhesion forces between foulants, leading to dense cake layers that are difficult to remove. The presence of divalent cations like Ca^{2+} facilitates bridging between organic and particulate foulants, promoting fouling severity.

Over the 120-min filtration, the UF permeate flux decreased from 22 to 5 L/(m^2·h), while NF flux dropped from 15.8 to 3 L/(m^2·h). Both PES-based UF and NF membranes experienced a similar flux decline of approximately 77–78%, despite their differing pore sizes. Although the relative decline is similar, the underlying fouling mechanisms likely differ. Studies indicate that UF membranes with larger pores are more susceptible to internal pore blocking by colloids and macromolecules, whereas NF membranes with smaller pores are more affected by surface fouling from particulate and organic matter. The RO membrane flux decreased from 3.8 to 3.0 L/(m^2·h), showing an absolute reduction and a notable change over the short-term test. PA-based RO membranes usually possess a dense, highly cross-linked PA active layer (as seen in Figure 4(f)), which provides strong resistance against particulate and colloidal fouling, unlike the more porous PES membranes. However, the overall flux was low in this study, likely because the applied pressure (10–12 bar) was much lower than typical industrial RO operations at around 30 bar (Adam *et al.* 2018).

Scanning electron microscopic (SEM) images of the fouled RO membrane surface, taken at the same magnification and detector settings as the fresh membrane, reveal a smooth, film-like fouling layer that completely obscures the original pore structure (Figure 4(a)). In contrast, the fresh membrane displays clearly defined pores and textured surface features. The dark, homogenous regions on the fouled membrane shown in Figure 4(b) and 4(c) are indicative of organic fouling, while embedded particles suggest a mixed fouling layer. EDS images shown in Figure 5(a) and spectra shown in Figure 5(c) further support this interpretation. Distinct Ca and P peaks were detected only in the fouled membrane, indicating calcium phosphate scaling, while minor signals of iron, copper, and zinc in the spectra indicate the trace contamination. As EDS

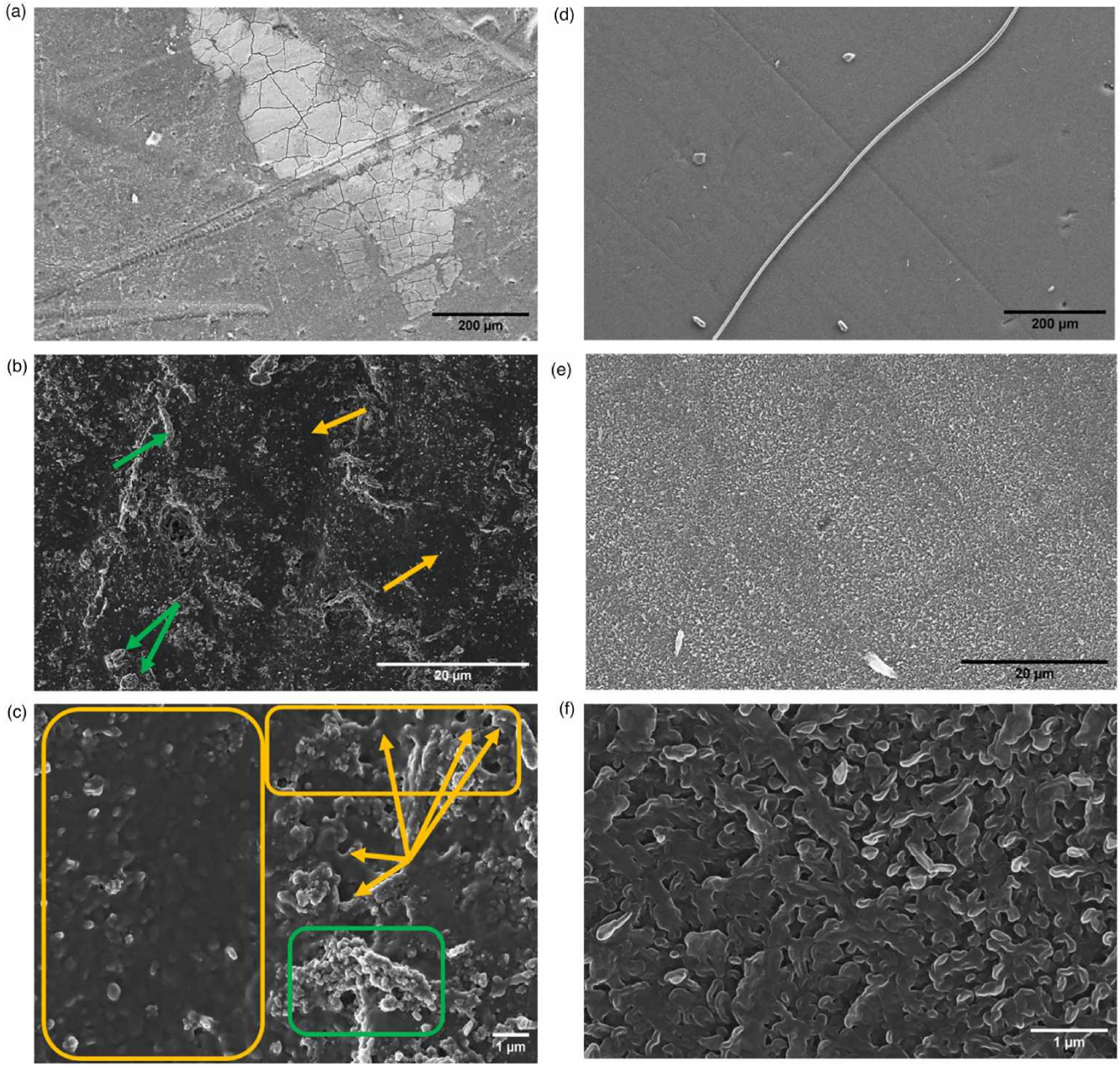

Figure 4 | SEM images comparing fouled (left) and fresh (right) PA-based RO membranes at different magnifications: (a) left: Fouled surface deposits; (b) left: organic fouling on smooth dark areas, (yellow arrows) and deposited particle (green arrow); (c) left: organic regions (yellow arrows), crystals or particle (green area).

cannot confirm organic matter due to the carbon coating of membrane samples for SEM, surface morphology becomes essential in identifying organic fouling. The presence of smooth surface areas lacking visible pores on the fouled RO membrane shown in Figure 4 supports this conclusion. In the context of pre-treatment, polyDADMAC was used as a flocculant during digestate dewatering, but no chloride (Cl) signals were detected in the EDS spectra, indicating either the absence of residual Cl in the permeate or a lack of interaction with membrane surface elements.

Importantly, calcium phosphate scaling is typically irreversible and often requires acidic or chemical cleaning (Mangal *et al.* 2021). In contrast, the organic fouling layer, although visually dominant in SEM, may be partially reversible, depending on its composition and bonding mechanisms. This is presented as a hypothesis, since no chemical cleaning specific to

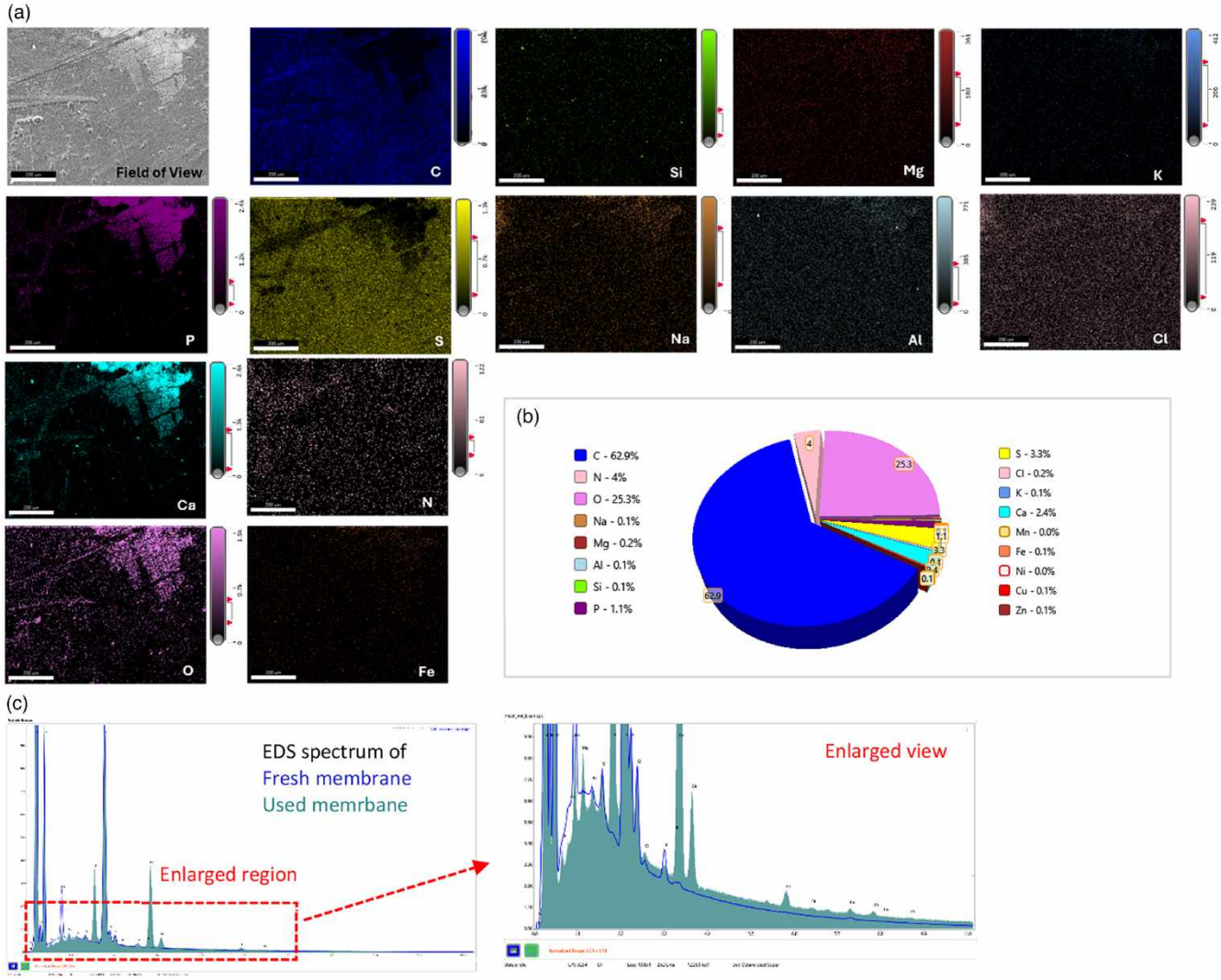

Figure 5 | (a) Mapping of fouled PA-based RO membrane showing the distribution and presence of key elements, (b) composition of elements on fouled PA-based RO membrane, and (c) EDS elemental spectra of fresh and fouled RO membrane.

organics (e.g., NaOH) or flux recovery measurements were performed. Additionally, as organic content cannot be quantified by EDS, this hypothesis is based solely on morphological evidence (e.g., smooth films and obscured pores). However, it is important to note that SEM and EDS analyses were conducted on a small section of the RO membrane, and the findings may not be representative of the entire membrane surface.

Following the batch tests, flux recovery was assessed by comparing the pure water permeate flux rate of UF, NF, and RO membranes before and after batch tests. The initial pure water flux values were 117.5 L/(m^2·h) for UF, 39 L/(m^2·h) for NF, and 7.8 L/(m^2·h) for RO (Figure 3(b)). After filtration, these values declined to 111, 35, and 7 L/(m^2·h), respectively, corresponding to flux recovery rates of 97% for UF and 91% for both NF and RO. These results suggest that UF experienced mainly reversible fouling, likely dominated by loosely bound particles and cake layers. In contrast, the only partial flux recovery of the RO membrane, along with SEM and EDS evidence, indicates a combination of organic fouling (partially reversible) and inorganic scaling (irreversible), particularly calcium phosphate. The initial pure water flux of the RO membrane was 7.8 L/(m^2·h), which decreased to 7.1 L/(m^2·h) after the batch test, corresponding to a flux recovery rate of 91%. As can be seen in the cake diagram of Figure 5(b), EDS analysis detected trace amounts of calcium (2.4%) and phosphate (1.1%) on the RO membrane. Although calcium phosphate is generally considered irreversible, the SEM morphology indicates loosely attached particulate scale rather than dense crystalline layers. It explains the observed flux loss from 3.8 to 3.0 L/(m^2·h) during

short-term operation in this study and did not cause a permanent flux decline. Manual cleaning removed part of these deposits under lab-scale conditions, although such removability cannot be assumed for industrial systems. This observation is limited to short-term laboratory operation and should not be extrapolated to long-term or full-scale systems, where calcium phosphate scaling is typically more persistent and difficult to remove.

The slightly lower recovery in NF and RO membranes also shows the presence of irreversible foulants or suboptimal cleaning protocols. Although the PA layer of RO membranes offers excellent resistance and rejection properties, it is still susceptible to persistent surface fouling under inadequate cleaning. Furthermore, denser membranes tend to accumulate more compact, less permeable fouling layers, which can limit recovery even after cleaning. These findings also highlight the influence of operating pressure. The applied pressure of 10–12 bar in this study is significantly lower than the industrial standards of 20–30 bar, potentially affecting both flux performance and the characteristics of the fouling layer (Zielińska & Mikucka 2021). A more aggressive cleaning strategy or operation under higher pressure might have improved flux recovery, especially for the RO membrane. These factors remain open to further investigation.

3.3. Pre-assessment of the economic view on water reuse from digestate in a model paper recycling mill

To reduce the freshwater demand and discharge volumes, this study initiated the pre-assessment of the potential for water reuse from the liquid fraction of anaerobically digested short-fiber residues in the model paper recycling mill-A (Figure 6).

The assessment is based on water quality obtained (Table 2) from this study and information provided by the paper recycling mills in Germany, with assumptions detailed in Table 3. Despite extensive internal recycling, most paper recycling mills continue to rely heavily on freshwater, particularly for high-quality applications such as paper formation, sealing water, and boiler feed. In the model paper recycling mill-A with a production capacity of 0.7 million t/a using 100% recovered paper, total freshwater demand is approximately 3 million m^3/a (4.4 m^3/t paper). Around 72% of this water is biologically treated on-site as part of the tertiary water circuit, involving anaerobic digestion followed by activated sludge treatment and secondary clarification to reduce COD levels. The treated water is then directed to the municipal treatment plant for further purification and discharge into water bodies. The remaining 28% water, i.e. 0.6 million m^3/a, constitutes net water consumption by the model paper mill, due to evaporation in the boilers, high contamination, or incorporation into the final paper product (Schoellershammer GmbH 2023). About 6–12% of the water is retained alone in the final paper product.

The large uncertainties in Ca^{2+}, Mg^{2+}, and total hardness explain the complex composition of the digestates. The digestates were mixtures derived from short-fiber residues supplied by multiple paper mills producing different paper products, resulting in variable mineral and organic contents. High DM (10 ± 3 wt%) and COD (41,435 ± 10,514 mg/L) indicate a heterogeneous matrix. pH (7.38 ± 0.17) and alkalinity may further influence Ca^{2+} and Mg^{2+} through carbonate equilibria. This heterogeneity propagates through downstream processes, such as solid–liquid separation and UF, so residual solids, organics, and minor pH/alkalinity variations in the liquid fraction and UF permeate contribute to the observed uncertainties.

Figure 6 shows the potential water circuit in the model paper recycling mill-A through water recovery from the digestate of short fiber residues. The paper recycling mill-A generates approximately 81,121 t/a of short-fiber residues (at 15% DM and 4% oDM), with a biogas potential of 0.4 m^3/kgoDM, corresponding to an energy yield of 6,490 MWh and a fuel capacity of 1 MW (at 5 kWh/Nm^3 for 50% CH_4). Integration of a combined heat power plant unit with ca. 220 kWel installed capacity and 40% electrical and 55% thermal efficiency would generate approximately 2,390 MWh of electricity and 2,560 MWh of heat annually. This equates to cost savings of 455,000 €/a for electricity (0.19€/kWh) and 204,800 €/a for heat (0.08€/kWh).

According to the oDM content and the biogas potential (0.4 Nm^3/kg oDM), only about 1,684 t/a of the short-fiber residues actually convert to biogas. Avoiding disposal of this fraction at 50 €/t results in a cost saving of approximately 84,200 €/a. The remaining mass after anaerobic digestion results in 79,434 t/a of digestate, composed of 80% water and 20% solids. Without any treatment, the entire digestate would require management. The solids fraction (15,887 t/a) would be disposed of as sludge at a cost amounting to 794,350 €/a. The liquid fraction (63,547 m^3/a) would be sent to municipal wastewater treatment plants at a typical fee of 1.3 €/m^3, resulting in a cost of 82,611 €/a. Thus, total untreated digestate management costs would amount to 876,961 €/a.

Applying RO treatment (e.g., SUEZ Proflex 12-2S unit) to the liquid fraction enables the recovery of up to 60% of water, equivalent to 38,128 m^3/a. This volume of recovered water avoids both freshwater procurement and wastewater discharge, translating into savings of 71,300 €/a for freshwater (at 1.87 €/m^3), and 49,566 €/a in avoided wastewater discharge fees (38,128 m^3 × 1.3 €/m^3). This results in combined savings of approximately 120,866 €/a from water recovery. However, the disposal of the remaining solid fraction still incurs a cost of 794,350 €/a. The electricity required to operate the RO

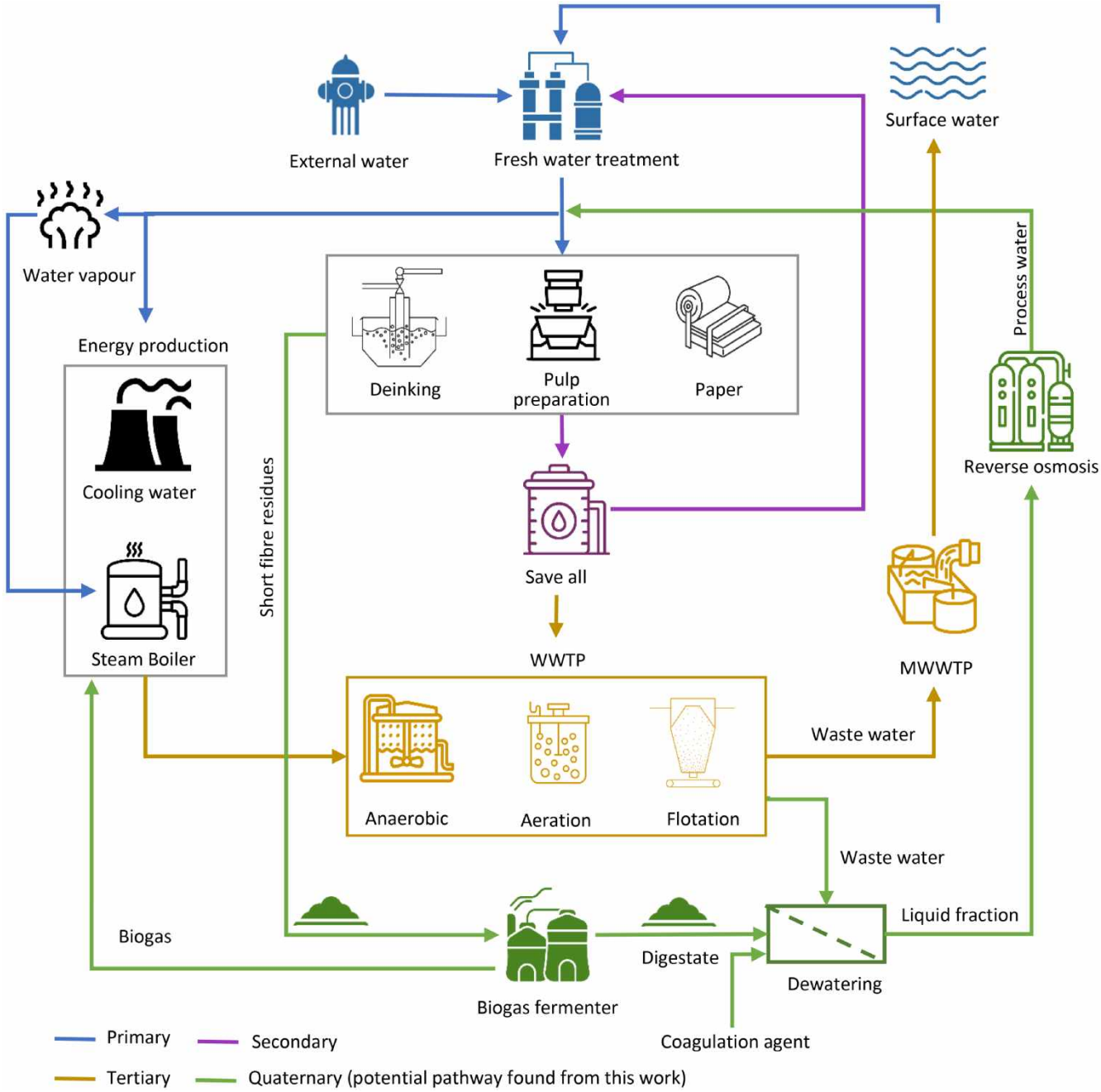

Figure 6 | Potential water circuit in a model paper recycling mill (icons from www.flaticon.com).

system adds another 63,547 € annually (1 kWh/m^3 wastewater). Overall, the combined savings from electricity (455,000 €/a) and heat (204,800 €/a) recovery through biogas production from short-fiber residues, including 84,200 €/a in avoided disposal costs for the 1,684 t/a of short fibers converted to biogas, along with savings of freshwater procurement (71,300 €/a) and avoided municipal wastewater treatment fees (49,566 €/a) through digestate water recovery, could total 0.86 million € annually for the model mill-A. After deducting residual disposal (794,350 €/a) and RO operational costs already discussed, the net savings are approximately 2,000 €/a, reflecting nearly cost-neutral.

Beyond digestate, the tertiary-treated effluent from the mill's biological wastewater treatment system presents another significant opportunity for water recovery. This effluent, accounting for 72% of the total wastewater volume, could be further

Table 2 | Permeate quality of UF, NF, and RO in this study with respect to water reuse in the paper mill

Parameter	Unit	Digestate[a]	Liquid fraction of digestate	Permeate UF	Permeate NF	Permeate UO	Fresh water standards in a paper mill
N_{tot}	mg/L	1,212 ± 316	484 ± 21	283 ± 105	278 ± 12	68 ± 5	–
NH_4-N	mg/L	560 ± 246	446 ± 45	336 ± 64	295 ± 10	58 ± 2	–
P_{tot}	mg/L	748 ± 316	32 ± 13	11 ± 8	<LOD[b]	<LOD	≤0.1
PO_4-P	mg/L	326 ± 138	17 ± 3	8 ± 2	<LOD	<LOD	–
Ca^{2+}	mg/L	492	197 ± 118	58 ± 27	15 ± 3	17 ± 4	≤75
Mg^{2+}	mg/L	610 ± 144.25	413 ± 202	65 ± 15	4 ± 3	20 ± 7	≤15
COD	mg/L	41,435 ± 10,514	1,456 ± 680	940 ± 212	106 ± 46	41 ± 14	≤30
DM	wt%	10 ± 3	0.4 ± 0.1	0.3 ± 0.01	<0.01	<0.01	
TDS	mg/L	3,102.90 ± 3,991	3,537 ± 145	<5,730	2,008 ± 38	335 ± 16	≤450
Colour	Pt-Co	–	413 ± 202	–	3 ± 2	3 ± 2	≤0.5
pH	–	7.38 ± 0.17	8 ± 0.4	8.1 ± 0.2	8.5 ± 0	8 ± 0.1	6.5–8
Total hardness	°dH	508.00 ± 390.32	43 ± 24	23 ± 17	3 ± 0	7 ± 2	≤14
EC[c]	µS/cm	11,850	6,848 ± 82	9,647 ± 1,810	4,025 ± 87	672 ± 38	≤900

[a]Liquid fraction of lab- and pilot-scale digestates.
[b]Method detection limit (LOD = 0.05 mg/L PO_4-P for LCK 349 and LOD = 2 mg/l PO_4-P for LCK 350).
[c]Electrical conductivity.

Table 3 | Assumptions of model paper recycling mill-A

Model paper recycling mill-A		Unit
Production capacity	700,000	t/a
Fresh water demand	3,092,034	m^3/a
Water consumption	773,009	m^3/a
Wastewater	2,215,925	m^3/a
Short fiber residues (SFR)	81,121	t/a
Biogas potential of SFR	0.4	Nm^3/kg oDM
Digestate from SFR	79,434	t/a
Water recovery through RO	33,362	m^3/a
Solids in digestate	15,887	t/a

polished using RO to produce high-quality water suitable for reuse across the mill. Full reuse of this stream could potentially replace up to 1.3 million m^3/a of freshwater demand, corresponding to savings of approximately 2.4 million €/a in freshwater procurement and 2.8 million €/a in wastewater discharge to municipal treatment facilities. However, implementing a near-closed water loop requires careful consideration. Zero-liquid-discharge concepts in paper recycling mills, such as in Zuelpich Mill of Kappa Paper, are well known, but they lead to operational issues such as $CaCO_3$ scaling (Han *et al.* 2021). Furthermore, RO systems also involve not only high energy demand but also chemical use and maintenance costs.

To ensure economic and technical feasibility, further development of low-cost, high-performance membranes and efficient cleaning strategies is needed. This economic pre-assessment highlights the potential for reducing environmental impact, saving water, and advancing circularity. However, a detailed life cycle assessment is needed to include investment, maintenance, chemical use, and other factors for a complete evaluation. Furthermore, RO for tertiary effluent remains to be investigated. Process-specific water quality demands must be matched to the recovered water to optimize reuse potential. The economic assessment presented here is preliminary and focuses on water recovery. A full evaluation, including zeolite integration, NH_4-N recovery, and associated CAPEX/OPEX, will be addressed in future work

3.4. Advanced NH_4-N recovery via hybrid RO and zeolite technology

NH_4-N removal and recovery were investigated using three hybrid scenarios integrating RO with natural zeolite-based ion exchange using clinoptilolite. Table 4 presents the characteristics of the influent and treated effluent streams by zeolite in each scenario. Figure 7 shows the percentage distribution of NH_4-N mass in each scenario, and Figure 8 presents the ion-exchange capacity of natural zeolite relative to NH_4-N mass in the treated stream.

For comparison purposes, the NH_4-N concentration in the digestate at the start of each scenario was considered as 100%, since initial concentrations varied among scenarios. In all three scenarios, about 2% of NH_4-N remained in the solid fraction after digestate dewatering. Since NH_4^+-N is mostly dissolved, this small portion likely comes from residual moisture held between solids in this laboratory case. In larger systems with better dewatering, this fraction would be expected to be negligible.

The clinoptilolite used contained 84% clinoptilolite, with minor minerals (plagioclase 3–4%, cristobalite 8%, rutile 0.1–0.3%, clay/mica 4%, trace quartz) that do not participate in ammonium ion exchange. While these minor minerals slightly dilute the effective cation exchange capacity per unit mass, the observed NH_4^+ adsorption shows the activity of the clinoptilolite fraction (Jha & Hayashi 2009). This occurs alongside influences from fouling, agglomeration, and competing cations.

Muscarella *et al.* (2021) used larger particles (2.0–2.5 mm) than here (0.05 mm), while Canellas *et al.* (2019) reported higher adsorption (17.1 and 20.7 mg NH_4-N/g clinoptilolite) using particles of 0.8–1.7 mm. Although smaller particles (0.05 mm) are usually better for adsorption, this was not observed in this study. We hypothesize that in this digestate matrix, the very fine particles (0.05 mm) tended to agglomerate, reducing the accessible surface area and masking exchange sites. Microscope images (Figure S4, Supplementary material) confirm extensive agglomeration of used zeolite compared with well-dispersed fresh particles. This agglomeration, together with fouling by organic matter and suspended solids, likely limited NH_4^+ access to exchange sites, resulting in the lower adsorption efficiency observed for the small particles.

The influence of competing cations on NH_4^+ adsorption is illustrated by the measured NH_4^+/Ca^{2+} and NH_4^+/Mg^{2+} ratios (Table 4). In Scenario 1, NH_4^+/Ca^{2+} dropped from 441 to 2.42 (182-fold decrease) and NH_4^+/Mg^{2+} from 1,324 to 8.51 (155-fold decrease). Scenario 2 showed a decrease from 29.79 to 6.90 (4.3-fold) for NH_4^+/Ca^{2+} and from 147.37 to 5.80 (25-fold) for NH_4^+/Mg^{2+}. Scenario 3 decreased from 188 to 2.71 (69-fold) for NH_4^+/Ca^{2+} and from 188 to 15.81 (12-fold) for NH_4^+/Mg^{2+}. These quantitative comparisons show that NH_4^+ adsorption is associated with simultaneous displacement of Ca^{2+} and Mg^{2+} from the zeolite. EDS elemental analysis of Scenario 1 (Table 1 in the Supplementary material) supports this, showing an increase in Ca (from 0.7 to 1.66 wt%) and Mg (from 0.3 to 0.44 wt%) on the zeolite after adsorption. Ca^{2+} shows the largest relative change in most scenarios. It has a stronger influence on NH_4^+ adsorption, but the exact effect is partly uncertain and varies depending on the feed composition.

RO retentate (Scenario 2) contained concentrated NH_4^+-N, multivalent cations (Ca^{2+}, Mg^{2+}), and organic matter, all competing for zeolite exchange sites. This is supported by observed reductions in electrical conductivity of up to 90% during

Table 4 | Characteristics of the influent and treated effluent streams of zeolite-adsorption

		Scenario 1	Scenario 2	Scenario 3	Scenario 1	Scenario 2	Scenario 3
		Influent			Treated effluent after zeolite-adsorption		
Parameter	Unit	LFD[a]	Retentate RO	Permeate RO	LFD	Retentate RO	Permeate RO
NH_4-N	mg/L	1,324	1,400	188	315 ± 16	290 ± 2	95 ± 9
Ca^{2+}	mg/L	3	47	<1	130 ± 5	42 ± 9	35 ± 4
Mg^{2+}	mg/L	<1	9.5	<1	37 ± 2	50 ± 1	6 ± 1
COD	mg/L	943	1,922	558	540 ± 3	753 ± 3	250 ± 5
pH	–	8.3			8.3 ± 0.3	7.6 ± 0.1	7.8 ± 0
Total hardness	°dH	<1	8.8	<1	27 ± 0	17 ± 1	5 ± 1
EC[a]	µS/cm		10.752	1,185	5,285 ± 36	1,305 ± 38	1,245 ± 67
NH_4^+/Ca^{2+}		441.3	29.79	188	2.42 ± 0.22	6.90 ± 1.53	2.71 ± 0.57
NH_4^+/Mg^{2+}		1,324	147.37	188	8.51 ± 0.89	5.80 ± 0.16	15.81 ± 4.14

[a]Liquid fraction of digestate.

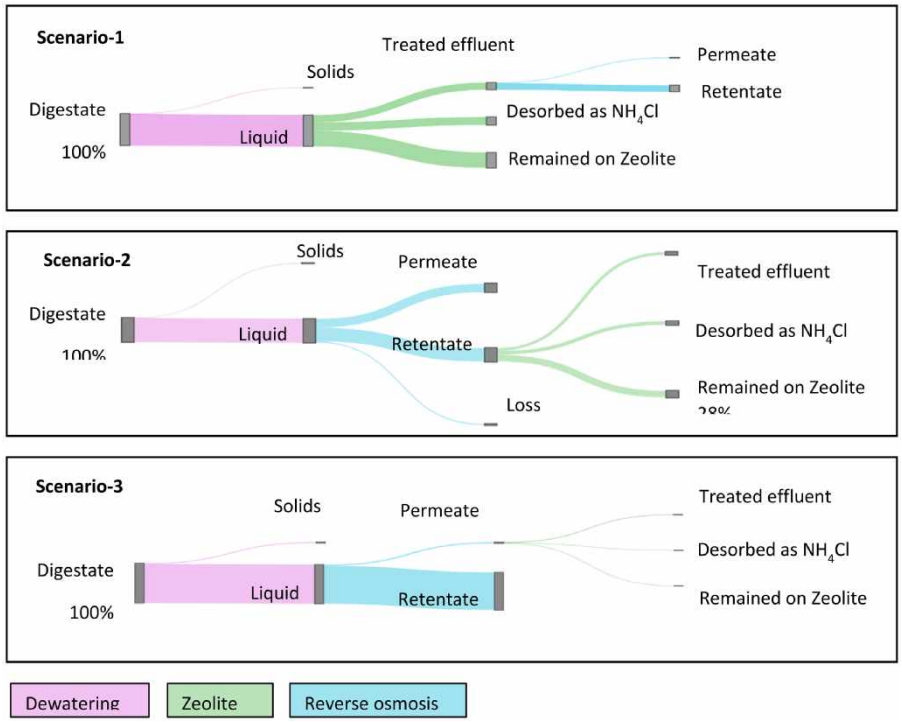

Figure 7 | Sankey diagram of mass (kg) distribution of NH_4-N, scenario (1): Zeolite and RO, (2) Retentate from RO and zeolite, (3) Permeate from RO and zeolite, made at SankeyMATIC.com.

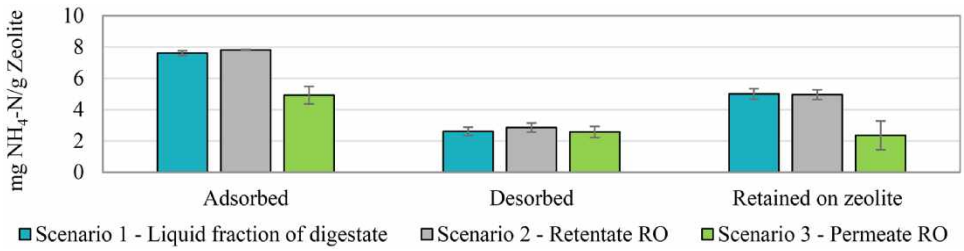

Figure 8 | Amount of NH_4-N adsorbed, desorbed, and retained on the natural zeolite-clinoptilolite during the treatment of the liquid fraction of digestate from the paper recycling process.

adsorption. It indicates simultaneous removal of multiple ionic species rather than NH_4^+ alone. COD removal (40% in Scenario 1, 55% in Scenario 2, and 70% in Scenario 3) likewise demonstrates co-adsorption or entrapment of organic constituents. Reported selectivity sequences (Hankins *et al.* 2005; Wang & Peng 2010) as well as the manufacturer's ranking for the zeolite used in this study ($Cs^+ > NH_4^+ > Pb^{2+} > K^+ > Na^+ > Ca^{2+} > Mg^{2+} > Ba^{2+} > Cu^{2+} > Zn^{2+}$) confirm that K^+, Ca^{2+}, and Mg^{2+} can outcompete NH_4^+ in complex wastewaters, further reducing adsorption efficiency.

Although Scenario 3 treated RO permeate with negligible Ca^{2+}, Mg^{2+}, electrical conductivity (1,185 μS/cm), and COD (558 mg/L), it showed the lowest adsorption efficiency (49%). This discrepancy is likely due to material-specific properties of the zeolite, such as its geological origin, which can influence ion-exchange capacity (Langwaldt 2008; Wang & Peng 2010). It suggests that solution composition alone does not fully determine adsorption efficiency and testing different zeolite sources could improve performance.

To directly verify the ion-exchange and fouling mechanisms suggested by solution chemistry, fresh, spent (after adsorption), and regenerated zeolite were analyzed via EDS (Figures S5–S7 in the Supplementary material). Clinoptilolite is a natural zeolite with a negatively charged framework that holds exchangeable cations, such as Na^+, K^+, Ca^{2+}, and Mg^{2+}. During NH_4^+ adsorption, ammonium ions can replace these cations at the zeolite surface. EDS analysis showed that Ca

and Mg on the zeolite surface increased from 0.72 and 0.34 wt% in the fresh zeolite to 1.66 and 0.46 wt% after adsorption. The simultaneous appearance of phosphorus (0.2 wt%) in localized spots that spatially overlapped with Ca-rich regions indicates the formation or deposition of calcium phosphate particles on the zeolite surface. This observation matches the same Ca-P clusters identified on the RO membrane surface. It explains that calcium phosphate precipitation occurred during treatment and contributed to surface fouling. At the same time, Ca^{2+} and Mg^{2+} concentrations in the effluent increased to over 100 mg/L (Scenario 1) and 35 mg/l (Scenario 3). This apparent contradiction can likely involve three processes: (i) displacement by NH_4^+, in which ammonium ions can push loosely bound Ca^{2+} and Mg^{2+} from weak sites on the zeolite into solution. The increase in Na on zeolite from 0.20 to 0.60 wt% (Table S1 in the Supplementary material) during adsorption confirms this ion-exchange activity, where some cations are redistributed rather than completely removed. (ii) Dissolution of solid Ca/Mg compounds: the digestate contains Ca and Mg in solid forms (e.g., carbonates or phosphates from Table 2) that partially dissolve in water, increasing effluent concentrations; and (iii) release from weakly bound surface sites: some Ca^{2+} and Mg^{2+} on the zeolite surface are not tightly incorporated into the crystal structure and can be released during NH_4^+ adsorption. However, it must be emphasized that NH_4^+ exchange cannot be directly confirmed via quantitative EDS. Nitrogen is not reliably detectable in standard EDS analysis, and any N signal must be manually forced into the quantification routine. Although localized N peaks were occasionally visible on the zeolite surface after adsorption (Figure S6 in the Supplementary material) and desorption, these signals are qualitative and not suitable for quantification. NH_4^+ uptake is therefore demonstrated by comparing NH_4^+ concentrations in the feed and the treated effluent after adsorption rather than through EDS. After desorption, Ca and Mg on the zeolite in this study slightly decreased to 1.56 and 0.38 wt%, while NH_4^+ removal remained substantial (Scenario 1 from 1,324 to 315 mg/L) and Scenario 3 from 188 to 95 mg/L, showing partial regeneration. These observations demonstrate that NH_4^+ adsorption involves simultaneous cation exchange with divalent ions. According to Hankins *et al.* (2005), the presence of competing cations can reduce ammonium uptake because zeolite preferentially adsorbs $K^+ > NH_4^+ > Na^+ > Ca^{2+}$, while Essington (2015) noted that ion-exchange in complex matrices often shows simultaneous uptake and release due to competition and matrix composition. Pre-treatment studies by Muscarella *et al.* (2021) show that pre-treatment of zeolite with NaCl or HCl can enhance NH_4^+ adsorption and minimize hardness. It should be noted that increased water hardness in the effluent is undesirable for paper industry reuse.

Trace heavy metals in the digestate (Table S2 in the Supplementary material), such as Zn^{2+}, Cu^{2+}, Pb^{2+}, and Ni^{2+}, may have further competed for binding sites or been released during NH_4-N adsorption (Blanchard *et al.* 1984; Aprianti *et al.* 2018). EDS analysis showed that Ni (0.3 wt%) was present on fresh zeolite and remained after adsorption but was no longer detected after desorption, indicating adsorption during the process and partial removal during regeneration. Cu and Zn were detected at trace levels in the liquid fraction of digestate and on fouled RO membranes (Figure 5). It explains limited adsorption and partial removal during desorption. Pb and Cd were present at very low concentrations in the digestate (<0.005 mg/L) and showed negligible uptake on the zeolite. These results highlight that, besides Ca^{2+} and Mg^{2+}, trace metals like Ni, Cu, and Zn contribute to the complexity of ion-exchange dynamics, though their adsorption is generally minor.

Desorption experiments achieved up to 52% NH_4-N recovery (Scenario 3) using a 30-fold Na^+ excess in the regenerant solution. To account for varying NH_4-N loadings, scenario-specific NaCl concentrations were applied: 46.5 g/L for Scenario 1, 204 g/L for Scenario 2, and 5 g/L for Scenario 3, corresponding to NaCl-to-NH_4-N ratios of 0.148, 0.703, and 0.053 mg NaCl/mg NH_4-N, respectively. It ensured proportional Na^+ and Cl^- availability for desorption, allowing comparable regeneration despite differing NH_4^+ loadings. Scenario 2 showed the highest ion-exchange capacity at 2.9 mg NH_4-N/g clinoptilolite, followed by Scenario 3 with 2.6 mg NH_4-N/g. Compared with previous studies, Wasielewski *et al.* (2017) achieved 75% desorption efficiency at a Na^+:NH_4^+ molar ratio of 30:1 using 2 g of zeolite, and Muscarella *et al.* (2021) reached 80% at 20:1 with 1 g zeolite. Although the same 30-fold molar ratio as Wasielewski *et al.* (2017) was applied, the larger zeolite masses in this study (80 g in Scenarios 1 and 2, 1.88 g in Scenario 3) and the fixed regenerant volume showed the lower desorption efficiency (maximum 52%). This indicates that regeneration process is influenced not only by the Na^+:NH_4^+ molar ratio but also by the zeolite-to-regenerant volume ratio. A detailed EDS-analysis were carried out for Scenario 1. During adsorption in Scenario 1, NH_4^+ should have replaced exchangeable cations such as K, Al, Si, and Ti in the zeolite, while residual Ca, Mg, and Na slightly increased during adsorption, as shown by EDS analysis. Moreover, Fe increased from 1.2 to 1.6% and P appeared at 0.2%, showing that these elements were temporarily adsorbed onto the zeolite surface during NH_4^+ uptake. During desorption, Na from the regenerant displaced NH_4^+ from the zeolite, and Cl^- entered the structure (from 0 to 1.1%) to maintain charge balance. The displaced NH_4^+ enters the solution, where it can

combine with Cl^- to form NH_4Cl, but no solid NH_4Cl forms inside the zeolite. During the desorption stage, K decreased to 1.9%, and Ca stabilized at 1.6%, indicating partial displacement of other cations. Fe and P decreased to 0.7 and 0%, respectively, indicating their removal during desorption. Si and Al also decreased, and carbon dropped from 34.2 to 10.2%, likely due to surface coverage and removal of organics. These results clearly demonstrate the ion-exchange dynamics, showing that NH_4^+ adsorption occurs via cation replacement, and desorption might have depended on Na^+/Cl^- availability and the zeolite-to-regenerant ratio. During adsorption, NH_4^+ should have replaced K, Ca, and other cations in the zeolite. EDS analysis show Na slightly increased from 0.2 to 0.6% after adsorption, reflecting residual Na^+ in the zeolite, while Cl remained at 0%. After desorption, Na remained at 0.5% and Cl increased to 1.1%, directly proving that Cl^- from the regenerant entered the zeolite to maintain charge balance during NH_4^+ displacement. K decreased from 2.9 to 1.9%, and Ca stabilized at 1.6%, showing partial displacement of other cations. Si and Al decreased, and carbon dropped from 34.2 to 10.2%, likely due to surface coverage and removal of organics. These observations confirm that NH_4^+ desorption depends on both Na^+/Cl^- availability and the zeolite-to-regenerant ratio.

4. CONCLUSIONS

The study confirms the technical feasibility of using membrane filtration for treating the liquid fraction of digestate from short-fiber residues. RO produced permeate meeting fresh water standards except for some NH_4-N. The low permeate yield of RO in this study was due to the limited pressure applied in lab tests and does not reflect industrial conditions. Membrane fouling remains a key scale-up concern under low-pressure conditions. The apparent removability of calcium phosphate scaling observed here is limited to short-term laboratory operation and should not be extrapolated to full-scale systems. Pilot trials using containerized RO units are therefore recommended. The preliminary assessment indicated that water recovery from digestate using RO can be nearly cost-neutral. However, a full life cycle and economic analysis is essential to confirm feasibility under industrial conditions.

This study confirmed that the complex matrix of industrial streams strongly affects the ion-exchange performance of natural clinoptilolite (zeolite). NH_4-N removal was measurable only in the more concentrated streams, while removal from RO permeate was negligible. High Ca^{2+} and Mg^{2+} concentrations released during adsorption limited the zeolite's suitability for water reuse in the paper industry, where low hardness is critical. Regeneration achieved only partial NH_4-N recovery, highlighting the need for optimization. Without modification or additional pre-/posttreatment, the tested natural clinoptilolite is not suitable as a standalone NH_4-N recovery step. The long-term stability should be addressed in future work.

ACKNOWLEDGEMENT

The authors would like to sincerely thank the paper companies and their representatives for their long-term cooperation, for sharing essential data on water quality standards, and for providing short-fiber residues for the research at FH Aachen.

This work contains results obtained from the experiments performed at the Ernst Ruska-Centre (ER-C) for Microscopy and Spectroscopy with Electrons at the Forschungszentrum Jülich (FZJ) in Germany. The ER-C beam-time access was provided via the project number ER-C E-065. The authors would like to extend thanks to ER-C for Microscopy and Spectroscopy with Electrons and the Jülich Centre for Neutron Science (JCNS-1), FZJ, for supporting the SEM- and EDS analysis conducted in this study. The icons used in Figure 4 in this manuscript were sourced from Flaticon.com and created by Aswell Studio, Designing Hub, Freepik. Cah nggunung, Alla Afanasenko, Uniconlabs, Three musketeers, Candy Design, Elastic1, bsd, Iconcity, and Ylivdesign.

FUNDING

This study was part of the doctoral research project. The project is supported by the Bauhaus-Universität Weimar with a scholarship within the framework of 'Thuringian graduate promotion'. The research work was conducted in cooperation with the FH Aachen University of Applied Sciences.

AUTHOR CONTRIBUTION

Conceptualization: D.W., M.G. Methodology: D.W., J.P., M.G., B.F. Formal analysis and investigation: D.W., B.J., B.F., J.P. Writing – original draft preparation: D.W. Writing – review and editing: D.W., S.K., J.P., M.G., S.B., B.F. Funding acquisition:

Bauhaus University Weimar. Resources: FH Aachen. Supervision: J.P., M.G., S.B. All authors have read and agreed to the published version of the manuscript.

DATA AVAILABILITY STATEMENT

Data cannot be made publicly available; readers should contact the corresponding author for details.

CONFLICT OF INTEREST

The authors declare there is no conflict.

REFERENCES

Adam, G., Mottet, A., Lemaigre, S., Tsachidou, B., Trouvé, E. & Delfosse, P. (2018) Fractionation of anaerobic digestates by dynamic nanofiltration and reverse osmosis: an industrial pilot case evaluation for nutrient recovery, *Journal of Environmental Chemical Engineering*, **6** (5), 6723–6732. https://dx.doi.org/10.1016/j.jece.2018.10.033.

Al Dwairi, R., Omar, W. & Al-Harahsheh, S. (2015) Kinetic modelling for heavy metal adsorption using Jordanian low cost natural zeolite (fixed bed column study), *Journal of Water Reuse and Desalination*, **5** (2), 231–238. https://dx.doi.org/10.2166/wrd.2014.063.

Amare, D. E., Ogun, M. K. & Körner, I. (2019) Anaerobic treatment of deinking sludge: methane production and organic matter degradation, *Waste Management*, **85**, 417–424. https://dx.doi.org/10.1016/j.wasman.2018.12.046.

Anari, Z., Morrissey, K., Kékedy-Nagy, L., Daneshpour, R., Abolhassani, M., Moore, J., Thoma, G. & Greenlee, L. (2023) Pressure-driven membrane nutrient preconcentration for down-stream electrochemical struvite recovery, *Separation and Purification Technology*, **309**, 122907. https://dx.doi.org/10.1016/j.seppur.2022.122907.

Aprianti, T., Miskah, S., Selpiana, Komala, R. & Hatina, S. (2018) Heavy metal ions adsorption from pulp and paper industry wastewater using zeolite/activated carbon-ceramic composite adsorbent, *Proceedings of the 17th International Conference on Ion Sources*. Geneva, Switzerland, 15–20 September 2017. p. 20127.

Aydın Temel, F. & Kuleyin, A. (2016) Ammonium removal from landfill leachate using natural zeolite: kinetic, equilibrium, and thermodynamic studies, *Desalination and Water Treatment*, **57** (50), 23873–23892. https://dx.doi.org/10.1080/19443994.2015.1136964.

Bareha, Y., Faucher, J.-P., Michel, M., Houdon, M. & Vaneeckhaute, C. (2022) Evaluating the impact of substrate addition for anaerobic co-digestion on biogas production and digestate quality: the case of deinking sludge, *Journal of Environmental Management*, **319**, 115657. https://dx.doi.org/10.1016/j.jenvman.2022.115657.

Blanchard, G., Maunaye, M. & Martin, G. (1984) Removal of heavy metals from waters by means of natural zeolites, *Water Research*, **18** (12), 1501–1507. https://dx.doi.org/10.1016/0043-1354(84)90124-6.

Canellas, J., Soares, A. & Jefferson, B. (2019) *Removing Ammonia From Wastewater Using Natural and Synthetic Zeolites: A Batch Experiment*. Cambridge, UK: ChemRxiv Preprint. ChemRxiv. https://doi.org/10.26434/chemrxiv.9831542.v1.

Cayé, N., Marasus, S. & Schüler, K. (2021) *Aufkommen und Verwertung von Verpackungsabfällen in Deutschland im Jahr 2021: Abschlussbericht (Generation and Recovery of Packaging Waste in Germany in 2021: Final report). Project No. 172078 (FB001331)*. Dessau-Roßlau, Germany: Umweltbundesamt. Available at: https://www.umweltbundesamt.de/sites/default/files/medien/11850/publikationen/162_2023_texte_aufkommen_verpackungsabfaelle.pdf (accessed 05 March 2025).

CEPI (2021) Key statistics 2021, Brussels: Confederation of European Paper Industries (CEPI). Available at: https://www.cepi.org/wp-content/uploads/2022/07/Key-Statistics-2021-Final.pdf.

CEPI (2024) Key statistics 2023, Brussels: Confederation of European Paper Industries (CEPI). Available at: https://www.cepi.org/wp-content/uploads/2024/09/Key-Statistics-2023-Final-2.pdf.

Cheenakula, D., Hilmi, R., Semchuk, I., Pettrak, J., Kuperjans, I., Grömping, M. & Beier, S. (2025) Investigation of particle size distribution and ultrafiltration of digestates from short- residues in paper mills, *Water Reuse*, **15** (1), 39–55. https://dx.doi.org/10.2166/wrd.2024.073.

Cséfalvay, E., Imre, P. & Mizsey, P. (2008) Applicability of nanofiltration and reverse osmosis for the treatment of wastewater of different origin, *Open Chemistry*, **6** (2), 277–283. https://dx.doi.org/10.2478/s11532-008-0026-3.

Digested Organics LLC (2020) *Food Waste Digestate Treatment with Multi-Stage Filtration*. Available at: https://digestedorganics.com/case-study/food-waste-digestate/ (accessed 6.05.2025).

European Environment Agency (EEA) (2022) *Share of energy consumption from renewable sources in Europe*. Copenhagen: European Environment Agency. Available at: https://www.eea.europa.eu/en/analysis/indicators/share-of-energy-consumption-from (accessed 05 March 2025)

Essington, M. E. (2015) *Soil and Water Chemistry*: An Integrative Approach, 2nd edn. Boca Raton, FL: CRC Press.

Faubert, P., Bélisle, C. L., Bertrand, N., Bouchard, S., Chantigny, M. H., Paré, M. C., Rochette, P., Ziadi, N. & Villeneuve, C. (2019) Land application of pulp and paper mill sludge may reduce greenhouse gas emissions compared to landfilling, *Resources, Conservation and Recycling*, **150**, 104415. https://dx.doi.org/10.1016/j.resconrec.2019.104415.

Foorginezhad, S., Zerafat, M. M., Ismail, A. F. & Goh, P. S. (2025) Emerging membrane technologies for sustainable water treatment: a review on recent advances, *Environmental Science: Advances*, **4** (4), 530–570. https://dx.doi.org/10.1039/D4VA00378K.

Fujioka, T., Kodamatani, H., Nghiem, L. D. & Shintani, T. (2019) Transport of N -Nitrosamines through a reverse osmosis membrane: role of molecular size and nitrogen atoms, *Environmental Science & Technology Letters*, **6** (1), 44–48. https://dx.doi.org/10.1021/acs.estlett.8b00624.

German Federal Environment Agency (2022) Altpapier (Waste paper). Available at: https://www.umweltbundesamt.de/daten/ressourcen-abfall/verwertung-entsorgung-ausgewaehlter-abfallarten/altpapier#die-deutsche-papierindustrie.

German Federal Office of Justice (2019) *Verordnung über das Inverkehrbringen von Düngemitteln, Bodenhilfsstoffen, Kultursubstraten und Pflanzenhilfsmitteln1 (Ordinance on the Marketing of Fertilisers, Soil Additives, Cultivation Substrates and Plant Aids1), (Düngemittelverordnung – DüMV)*. Federal Law Gazette I, 2012, p. 2482. Available at: https://www.gesetze-im-internet.de/d_mv_2012/BJNR248200012.html (accessed 05 March 2025).

Gienau, T., Brüß, U., Kraume, M. & Rosenberger, S. (2018) Nutrient recovery from anaerobic sludge by membrane filtration: pilot tests at a 2.5 MWe biogas plant, *International Journal of Recycling of Organic Waste in Agriculture*, **7** (4), 325–334. https://dx.doi.org/10.1007/s40093-018-0218-6.

Giuntoli, J., Agostini, A., Edwards, R. & Marelli, L. (2015) *Solid and gaseous bioenergy pathways: input values and GHG emissions: calculated according to the methodology set in COM(2016) 767*. Luxembourg: Publications Office, European Commission (Publisher), Joint Research Centre. EUR 27215 EN. Available at: https://data.europa.eu/doi/10.2790/27486 (accessed 05 March 2025)

Guida, S., Potter, C., Jefferson, B. & Soares, A. (2020) Preparation and evaluation of zeolites for ammonium removal from municipal wastewater through ion exchange process, *Scientific Reports*, **10** (1), 12426. https://dx.doi.org/10.1038/s41598-020-69348-6.

Hafiz, M., Hawari, A. H., Alfahel, R., Hassan, M. K. & Altaee, A. (2021) Comparison of nanofiltration with reverse osmosis in reclaiming tertiary treated municipal wastewater for irrigation purposes, *Membranes*, **11** (1), 32. https://dx.doi.org/10.3390/membranes11010032.

Hajduk, A., Dębowski, M., Zieliński, M. & Rusanowska, P. (2017) The utilisation of zeolites for the reduction of ammonium concentration in biogas processes, *Technical Transactions*, **114** (11), 107–116. https://doi.org/10.4467/2353737XCT.17.195.7424.

Han, N., Zhang, J., Hoang, M., Gray, S. & Xie, Z. (2021) A review of process and wastewater reuse in the recycled paper industry, *Environmental Technology & Innovation*, **24**, 101860. https://dx.doi.org/10.1016/j.eti.2021.101860.

Hankins, N. P., Pliankarom, S. & Hilal, N. (2005) An equilibrium ion-exchange study on the removal of NH 4+ ion from aqueous effluent using clinoptilolite, *Separation Science and Technology*, **39** (15), 3639–3663. https://dx.doi.org/10.1081/SS-200038180.

Huang, Z., Cui, W., Liu, W., Xia, R., Cao, D., Ding, X., Li, G. & Luo, W. (2023) Effects of membrane pore size on nutrient enrichment and membrane fouling behavior in nanofiltration of ultrafiltration permeate from biogas slurry concentration, *Transactions of the Chinese Society of Agricultural Engineering*, **39** (8), 205–214. https://doi.org/10.11975/j.issn.1002-6819.202212189.

Jha, V. K. & Hayashi, S. (2009) Modification on natural clinoptilolite zeolite for its NH4 + retention capacity, *Journal of Hazardous Materials*, **169** (1–3), 29–35. https://dx.doi.org/10.1016/j.jhazmat.2009.03.052.

Kaya, Y. & Dayanir, S. (2020) Application of nanofiltration and reverse osmosis for treatment and reuse of laundry wastewater, *Journal of Environmental Health Science & Engineering*, **18** (2), 699–709. https://dx.doi.org/10.1007/s40201-020-00496-7.

Kotoulas, A., Agathou, D., Triantaphyllidou, I. E., Tatoulis, T. I., Akratos, C. S., Tekerlekopoulou, A. G. & Vayenas, D. V. (2019) Zeolite as a potential medium for ammonium recovery and second cheese whey treatment, *Water*, **11** (1), 136. https://dx.doi.org/10.3390/w11010136.

Langwaldt, J. (2008) Ammonium removal from water by eight natural zeolites: a comparative study, *Separation Science and Technology*, **43** (8), 2166–2182. https://dx.doi.org/10.1080/01496390802063937.

Leca, M.-A., Regnault, L., Sambusiti, C., Monlau, F., Le Guer, Y. & Beigbeder, J.-B. (2024) Treating liquid anaerobic digestate using natural zeolite and *Arthrospira platensis* cyanobacteria: from laboratory to pilot-scale, *Chemical Engineering Journal Advances*, **20**, 100660. https://dx.doi.org/10.1016/j.ceja.2024.100660.

Leiviskä, T., Nurmesniemi, H., Pöykiö, R., Rämö, J., Kuokkanen, T. & Pellinen, J. (2008) Effect of biological wastewater treatment on the molecular weight distribution of soluble organic compounds and on the reduction of BOD, COD and P in pulp and paper mill effluent, *Water Research*, **42** (14), 3952–3960. https://dx.doi.org/10.1016/j.watres.2008.06.016.

Liu, G., Yu, S., Yang, H., Hu, J., Zhang, Y., He, B., Li, L. & Liu, Z. (2016) Molecular mechanisms of ultrafiltration membrane fouling in polymer-flooding wastewater treatment: role of ions in polymeric fouling, *Environmental Science and Technology*, **50** (3), 1393–402. https://doi.org/10.1021/acs.est.5b04098. PMID: 26735590

Liu, S., Foo, Z. H., Lienhard, J. H., Keten, S. & Lueptow, R. M. (2025) Membrane charge effects on solute transport in nanofiltration: experiments and molecular dynamics simulations, *Membranes*, **15** (6), 184. doi: 10.3390/membranes15060184

Ma, Z., Zhang, Q., Weng, X., Mang, C., Si, L., Guan, Z. & Cheng, L. (2018) Fluoride ion adsorption from wastewater using magnesium(II), aluminum(III) and titanium(IV) modified natural zeolite: kinetics, thermodynamics, and mechanistic aspects of adsorption, *Journal of Water Reuse and Desalination*, **8** (4), 479–489. https://dx.doi.org/10.2166/wrd.2017.037.

Maghfiroh, M., Park, N. R., Chang, H. Y., Jung, J. H., Ahn, K. H., Lim, H. M. & Kim, W. J. (2023) Ammonium removal and recovery using natural zeolites and air stripping technique for greywater treatment, *International Journal of Environmental Science and Technology*, **20** (5), 4931–4942. https://dx.doi.org/10.1007/s13762-022-04285-7.

Mai, Z., Shi, Y., Li, B., Han, S., Sun, Y., Zhu, H., Xu, P., Hu, M., Yoshioka, T. & Matsuyama, H. (2025) Multiscale insights into polyamide membrane fouling during reverse osmosis of rare earth wastewater, *Journal of Membrane Science*, **715**, 123445. https://dx.doi.org/10.1016/j.memsci.2024.123445.

Mangal, M. N., Salinas-Rodriguez, S. G., Dusseldorp, J., Kemperman, A. J., Schippers, J. C., Kennedy, M. D. & van der Meer, W. G. (2021) Effectiveness of antiscalants in preventing calcium phosphate scaling in reverse osmosis applications, *Journal of Membrane Science*, **623**, 119090. https://dx.doi.org/10.1016/j.memsci.2021.119090.

Muscarella, S. M., Badalucco, L., Cano, B., Laudicina, V. A. & Mannina, G. (2021) Ammonium adsorption, desorption and recovery by acid and alkaline treated zeolite, *Bioresource Technology*, **341**, 125812. https://dx.doi.org/10.1016/j.biortech.2021.125812.

Omar, W. S. (2015) Treatment of wastewaters contaminated with zinc ions using natural zeolite as adsorbent in a fixed bed column, *Journal of Water Reuse and Desalination*, **5** (4), 542–549. https://dx.doi.org/10.2166/wrd.2015.032.

Schoellershammer GmbH (2023) *Sustainability Report Schoellershammer 2023* (Sustainability report). Düren, Germany: Schoellershammer GmbH. Available at: https://www.schoellershammer.de/wp-content/uploads/2024/12/SCHOELLERSHAMMER-NHB-2023-1.pdf (Accessed: 25.06.2025).

Steffen, F., Janzon, R., Wenig, F. & Saake, B. (2017) Valorization of waste streams from deinked pulp mills through anaerobic digestion of deinking sludge, *BioResources*, **12** (3), 4547–4566. https://dx.doi.org/10.15376/biores.12.3.4547-4566.

Tarpeh, W. A., Udert, K. M. & Nelson, K. L. (2017) Comparing ion exchange adsorbents for nitrogen recovery from source-separated urine, *Environmental Science & Technology*, **51** (4), 2373–2381. https://dx.doi.org/10.1021/acs.est.6b05816.

Wang, S. & Peng, Y. (2010) Natural zeolites as effective adsorbents in water and wastewater treatment, *Chemical Engineering Journal*, **156** (1), 11–24. https://dx.doi.org/10.1016/j.cej.2009.10.029.

Wasielewski, S., Morandi, C., Minke, R. & Steinmetz, H. (2017) *Ammoniumrückgewinnung durch Ionenaustausch mittels Zeolith (Ammonium recovery by ion exchange using zeolite)*. University of Stuttgart, Stuttgart (City), Germany: Institute for Sanitary Engineering, Water Quality and Solid Waste Management. Available at: https://www.isi.fraunhofer.de/content/dam/isi/dokumente/ccn/twist/ergebnispapiere/technologien/Ammoniumrueckgewinnung.pdf (Accessed: 25.06.2025).

Zhang, X., Li, X., Zhang, F., Peng, S., Tumrani, S. H. & Ji, X. (2019) Adsorption of Se(IV) in aqueous solution by zeolites synthesized from fly ashes with different compositions, *Journal of Water Reuse and Desalination*, **9** (4), 506–519. https://dx.doi.org/10.2166/wrd.2019.036.

Zhang, T., Zhang, W. & Sun, P. (2024) Potassium and ammonium recovery in treated urine by zeolite based mixed matrix membranes, *Journal of Environmental Management*, **368**, 122169. https://dx.doi.org/10.1016/j.jenvman.2024.122169.

Zielińska, M. & Mikucka, W. (2021) Membrane filtration for valorization of digestate from the anaerobic treatment of distillery stillage, *Desalination and Water Treatment*, **215**, 60–68. https://dx.doi.org/10.5004/dwt.2021.26772.

First received 29 July 2025; accepted in revised form 24 February 2026. Available online 7 March 2026